www.rsc.org/pccp

PAPER

Visible luminescence spectroscopy of free-base and zinc phthalocyanines isolated in cryogenic matrices†

Ciaran Murray,‡[a] Nadia Dozova,§[a] John G. McCaffrey,*[a] Niloufar Shafizadeh,[b] Wuthurath Chin,[b] Michel Broquier[b] and Claudine Crépin*[b]

Received 22nd June 2011, Accepted 11th August 2011
DOI: 10.1039/c1cp22039j

The absorption, emission and excitation spectra of ZnPc and H_2Pc trapped in Ne, N_2, Ar, Kr and Xe matrices have been recorded in the region of the Q states. A comparison of the matrix fluorescence spectra with Raman spectra recorded in KBr pellets reveals very strong similarities. This is entirely consistent with the selection rules and points to the occurrence of only fundamental vibrational transitions in the emission spectra. Based on this behaviour, the vibronic modes in emission have been assigned using results obtained recently on the ground state with large basis-set DFT calculations [Murray *et al. PCCP*, **12**, 10406 (2010)]. Furthermore, the very strong mirror symmetry between excitation and emission has allowed these assignments to be extended to the excitation (absorption) bands. While this approach works well for ZnPc, coupling between the band origin of the $S_2(Q_Y)$ state and vibrationally excited levels of $S_1(Q_X)$, limits the range of its application in H_2Pc. The Q_X/Q_Y state coupling is analysed from data obtained from site-selective excitation spectra, revealing pronounced matrix and site effects. From this analysis, the splitting of the Q_X and Q_Y states has been determined more accurately than in any previous attempts.

I. Introduction

As a result of considerable interest in the phthalocyanines[1] (Pcs) as potential photo-conductors[2] or as nonlinear materials,[3] the optical properties of free-base phthalocyanine (H_2Pc) and zinc phthalocyanine (ZnPc) have been studied in a wide range of environments. Thus the electronic spectroscopy of both molecules have been reported in the gas phase,[4,5] in low-temperature jets,[6–8] in He droplets[9,10] and in thin films.[11] The two molecules have also been studied in cryogenic matrices: either in Shpol'skii organic matrices[12–14] or isolated in the solid rare gases.[15–18] In a detailed magnetic circularly polarised luminescence (MCPL) study of ZnPc, Schatz and co-workers[19] identified the presence of both crystal field splitting and Jahn–Teller coupling on the degenerate first excited singlet state. IR and Raman spectra for H_2Pc in thin films[20] and for ZnPc in KBr discs[21] have been presented and theoretical predictions for both molecules have also been published.[22,23] Recently we have used the matrix-isolation technique to obtain vibrational signatures of both molecules,[24] free of spectral complexities due to aggregates. With the input of large basis-set density functional theory (DFT) calculations, we have achieved a comprehensive vibrational analysis[24] of the matrix spectra of both molecules.

In contrast to the porphyrins, the transition between the ground state $G(S_0)$ and the first excited singlet $Q(S_1)$ state is fully allowed in the phthalocyanines. This transition is responsible for the intense Q-band absorption in the red part of the spectrum. For a molecule like ZnPc with D_{4h} symmetry, the S_1 state is degenerate, while in H_2Pc, having D_{2h} symmetry, the degeneracy is lifted and two states arise—labelled the $Q_X(S_1)$ at lower energy and the $Q_Y(S_2)$ at higher energy. The resulting strong absorption in the 600–850 nm range—the so-called therapeutic body window—renders the phthalocyanines especially relevant for medical applications as photosensitisers in laser cancer therapy.[25]

The most recent laser-induced fluorescence (LIF) investigation of zinc and free-base phthalocyanine made under jet-cooled conditions has been reported by Plows and Jones.[6] In spite of numerous gas phase studies of H_2Pc, the band origin of the $Q_Y(S_2)$ state has still not been conclusively determined. This is due to the spectral complexity which arises from the coupling between the band origin of the $Q_Y(S_2)$ state and the high frequency modes of the $Q_X(S_1)$ state. Matrix-isolation spectroscopy affords an ideal opportunity to identify the true band

[a] *Department of Chemistry, National University of Ireland – Maynooth, Co. Kildare, Ireland. E-mail: john.mccaffrey@nuim.ie*
[b] *Institut des Sciences Moléculaires d'Orsay UMR 8214 – Univ. Paris-Sud, CNRS, Orsay, F-91405 France. E-mail: claudine.crepin-gilbert@u-psud.fr*

† Electronic supplementary information (ESI) available. See DOI: 10.1039/c1cp22039j

‡ Present address: Tyndall National Institute, University College Cork, "Lee Maltings", Dyke Parade, Cork, Ireland.

§ Present address: Laboratoire P.A.S.T.E.U.R. -UMR 8640, Ecole Normale Superieure, Paris, France.

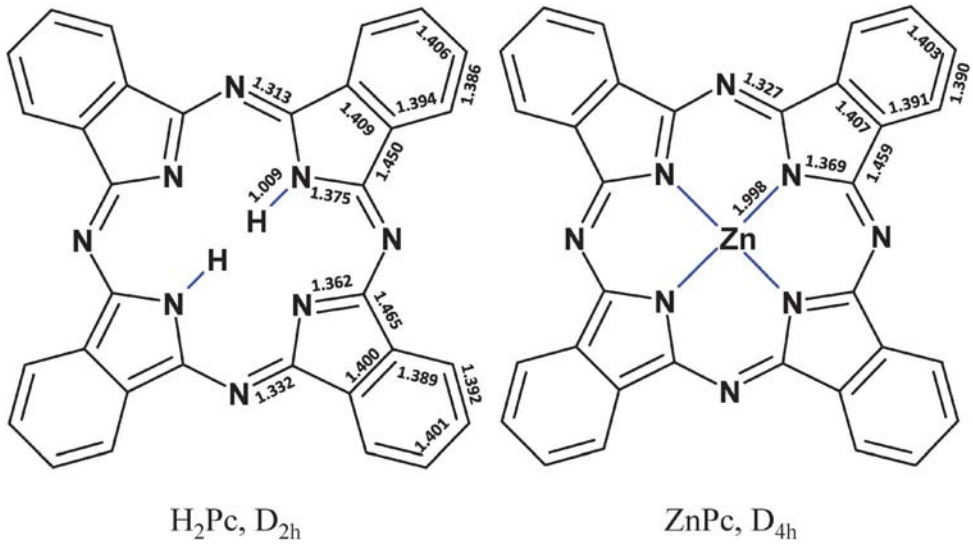

Fig. 1 Structures of ZnPc [D_{4h}] and H_2Pc [D_{2h}] determined by the recent large basis-set DFT calculations presented in ref. 24.

origin since spectra recorded under these conditions are free of any rotational structure and solvent-shifts induced by the solid rare gases, while present, are small and can be used to monitor the effect of matrix shifts on the Q_X/Q_Y state couplings. Since the density of vibrational levels in $Q_X(S_1)$ is not very high in the region 1000 cm^{-1} above its origin, the coupling can vary strongly as a function of the host matrix. Because of slightly different shifts, it may also be dependent on the site occupied in a given host solid and will also be sensitive to isotopic substitution. For the aforementioned reasons, we undertook an investigation of the visible spectroscopy of H_2Pc and ZnPc isolated in inert, low temperature solids.

While H_2Pc belongs to the D_{2h} symmetry point group and ZnPc belongs to D_{4h}, both molecules are expected to have very similar geometries. As shown in Fig. 1, the structures determined by us in recent DFT calculations[24] confirm these expectations where the geometry optimised structures are presented for both molecules. The DFT calculations were conducted with the B3LYP functional and the large 6-311++G(2d,2p) basis set was used to predict the infrared and Raman frequencies. Complete details of the molecular parameters for both H_2Pc and ZnPc were provided in Table S1 of the supplementary material in ref. 24 while the predicted IR and Raman frequencies were given in Table S2.

Visible absorption spectra of H_2Pc and ZnPc isolated in a variety of matrices were first reported by Bajema *et al.*[17] A detailed lineshape analysis of H_2Pc in Ar has been presented by Geissinger *et al.*[26] The emission and excitation spectra of H_2Pc have been studied in Ar matrices by Bondybey and English.[18] In contrast, the Ne and N_2 systems have not yet received much attention. Like the porphyrins, the phthalocyanines have a propensity of forming aggregates in more concentrated matrix samples. As demonstrated in the systematic matrix study of Williamson and co-workers[16] on ZnPc, such species absorb to the red of the sharp 0–0 monomer Q state transitions. The content of aggregate species was kept to a minimum in the samples prepared in the present study. Accordingly, the absorption and emission spectra recorded herein correspond to samples containing well-isolated guest molecules.

In an earlier study conducted by us[27] it was noticed that one particular vibronic mode in the emission spectra of both ZnPc and H_2Pc exhibited very efficient stimulated emission (SE) when isolated in low temperature matrices and excited with a pulsed dye laser. The modes concerned were located at 1550 and 1525 cm^{-1} in H_2Pc and ZnPc respectively in Ar matrices. With increased laser intensity or in more concentrated samples, lower frequency modes also produced SE. The emission bands exhibiting this behaviour will be analysed in the present work to achieve vibrational assignments.

In the present paper we describe a study of the absorption and luminescence spectra of ZnPc and H_2Pc isolated in rare gas and nitrogen matrices in the region of the Q band. Very strong similarities were noted in our earlier study[24] between the vibrational structure in Raman and emission spectra. A key aspect of the present work is the exploitation of vibrational analysis[24] of Raman spectra, presented in ref. 24, to obtain assignments for the emission bands. Due to the strong mirror symmetry between emission and excitation spectra, an opportunity thereby exists to also achieve vibrational assignments for the multiple lines present in the excitation spectroscopy of the phthalocyanines. Moreover, detailed comparison of the recorded excitation and emission spectra aids considerably in the identification of the true band origin in the region of the onset of the $Q_Y(S_2)$ excited state of H_2Pc since the complicated excitation bandshapes presented in this spectral region can be isolated and then analysed.

II. Experimental

Experiments on free-base (H_2Pc) and zinc (ZnPc) phthalocyanines were undertaken at both the Institut des Sciences Moléculaires d'Orsay (ISMO) at Orsay and by the Low Temperature Spectroscopy (LTS) group at NUI-Maynooth. ZnPc and H_2Pc were purchased from Sigma Aldrich and Fluka respectively and used without further purification. Matrix samples were prepared by resistive heating of the phthalocyanines to around 350 °C using the flowing host gas to entrain the Pc vapour for deposition on a CaF_2 window

(sapphire at Orsay) at cryogenic temperatures. The oven design[28] used in both experiments has been described recently. The cryogenic set-ups used differ only in the minimum temperatures attainable with a base value of 7 K possible at Orsay while it is 13 K at Maynooth. Large gas flows (40 mmol/h) for a period of approximately 30 mins were required to achieve isolation of phthalocyanine (Pc) as a monomer for samples used to record visible spectroscopy. The isolation condition of the Pcs in matrices was monitored with absorption in the red region of the visible spectrum. For this a tungsten lamp source was used.

Luminescence (emission-excitation) spectra were recorded using tuneable dye lasers—either a home-built system at Orsay or the Quantel TDL90 system at Maynooth. The dyes DCM and LDS698 were used to cover the spectral ranges 625–660 nm and 665–685 nm respectively. Both systems are pumped by the second harmonic of nanosecond Q-switched Nd:YAG lasers that have been described previously.[29,30] Emission was recorded with the Andor DH720 intensified, time-gated charge coupled device (iCCD) detector system. Absorption and emission spectra were recorded on a 0.6 m Jobin-Yvon monochromator at Orsay (resolution of few cm^{-1}), while a 0.5 m Acton Research SP500i monochromator was used at Maynooth. Excitation spectra were recorded by varying the laser wavelength while monitoring a range of emission wavelengths with the iCCD camera. This technique allowed us to record high-resolution excitation spectra of several emission bands simultaneously. The resulting total luminescence, when presented in the form of 2D excitation-emission matrices (EEM) plots, provides a very powerful method of resolving complex site occupancy. No correction, including the spectral sensitivity of the detection system, was applied to the spectral data.

III. Results

1. Visible absorption

The absorption spectra of ZnPc in all matrices are dominated, as shown on the left panel in Fig. 2, by the intense 0–0 transition of the Q band. The band maximum of this transition has been observed in the gas phase under bulb[5] conditions at 15 128 cm^{-1} while the band origin has been identified at 15702.9 cm^{-1} in liquid helium droplets[10] and at 15 766 cm^{-1} in free jet[6] conditions. The last value is indicated by the dashed vertical line in Fig. 2. The 0–0 transition of the Q band is situated at 15 574, 15 328, 15 309, 15 182 and 15 035 cm^{-1} in Ne, N_2, Ar, Kr and Xe respectively. These bands are all red-shifted from the gas phase position and the energy of the transition decreases from Ne to Xe when the interaction with the matrix gets stronger. Thus the largest shift from the gas phase has been observed in Xe with a value of 731 cm^{-1} while the smallest is 192 cm^{-1} in neon. It is only 63 cm^{-1} in helium droplets.[10] Other vibronic bands of lower intensity are evident in the region from 15 500 to 17 000 cm^{-1}. The spectra in Ne and N_2 have been recorded at 8 K and these matrices, especially N_2, exhibit resolved site structure. The absorption spectra in Ar, Kr and Xe were recorded at higher temperature (13 K) and while the bands are broader, they do show resolved features in laser excitation scans.

In contrast to ZnPc, the absorption spectra of H_2Pc recorded at 8 K, appear more complex and structured as

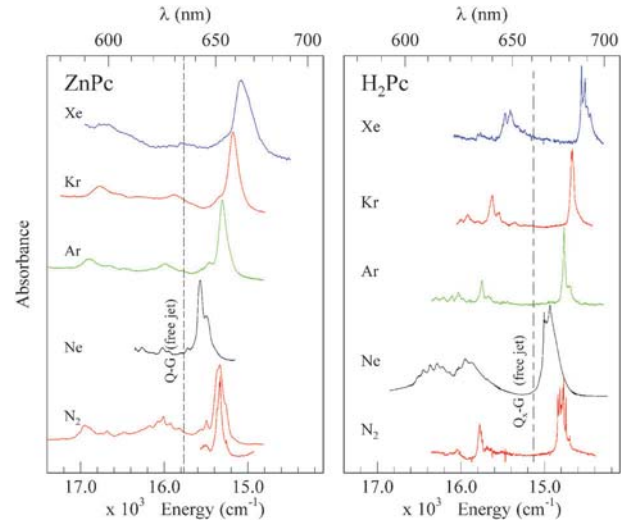

Fig. 2 Absorption spectra of ZnPc (left panel) and H_2Pc (right panel) trapped in Ne, N_2, Ar, Kr and Xe solids. All the spectra were recorded at 8 K except for ZnPc in N_2, Ar, Kr and Xe which were recorded at 13 K. The lower trace presented for ZnPc in N_2 was recorded at 8 K. The locations of the gas phase band origins which are accurately known from jet experiments are indicated by the dashed vertical lines.

shown on the right in Fig. 2. In addition, two principal features are evident in the spectra recorded in all samples corresponding to absorptions of the Q_X and Q_Y states. The band origin of the $Q_X(S_1) \leftarrow G(S_0)$ transition is known from laser excitation spectroscopy[7] done in jets to be 15 132 cm^{-1} in the gas phase and at 15088.9 cm^{-1} in helium droplets.[10] The absorption values recorded in all the matrices studied are collected in Table 1 as well as the matrix shifts. As indicated in Fig. 2 a red-shift exists in all matrices—it is smallest in Ne (198 cm^{-1}) and largest in Xe (573 cm^{-1}). The Q_Y–Q_X splitting is also host dependent, decreasing from Ne to Xe. In fact, the Q_Y-G transition energy is reduced by a very similar fraction as the Q_X-G transition energy in the different matrices (see Table 1).

In yet further contrast to ZnPc, the shapes of the H_2Pc bands differ markedly from one solid to another with a highly structured band present in N_2 and a broad but structured band in Ne. Ar presents the simplest absorption spectrum with a single dominating feature. However, as revealed in laser excitation spectroscopy, the widths of the bands in all matrices arise from occupancy of the H_2Pc or ZnPc molecules in multiple sites. However, in the case of H_2Pc/N_2, the resolved lines of the structured absorption band are very narrow and could arise from distinct sites. Their linewidths (4 to 5 cm^{-1}) are close to the resolving power of the recording instruments, $\sim$2 cm^{-1} in this case.

When isolated in solids, free-base phthalocyanine can exist in two distinct tautomeric forms which differ depending on the position of the two hydrogen atoms on the inner ring of the H_2Pc molecule. Because of the interaction with the host matrix, these two tautomers are known from existing matrix work[31] on free-base porphine to have different absorption frequencies. Thus, where only one band appears in the ZnPc absorption spectrum, two are expected for H_2Pc. This fact can explain why some of the absorptions peaks of free-base

Table 1 Absorption values in wavenumbers (cm^{-1}) units for the band origins of ZnPc (Q band) and H_2Pc (Q_X) in different matrices as determined from the band maxima. The gas phase band origins are from the published data of Fitch *et al.* [ref. 7] for H_2Pc and from Plows and Jones [ref. 6] for ZnPc. The splitting of the Q_X and Q_Y matrix bands of H_2Pc determined in this way (from absorption spectra) are only rough indicators of the splitting. Much more precise, site specific values emerge from a detailed analysis of site-resolved excitation data discussed in Section IV.C.2. The helium data is from the work of Lehning *et al.* [ref. 10], while the Shpol'skii data is that of Huang *et al.* [ref. 13]. The gas phase and liquid helium splittings quoted (highlighted by asterisks) are estimates based on band assignments emerging in the analysis conducted in the present study

	H_2Pc				ZnPc	
	Q_X	Matrix shift	Q_Y	Q_Y–Q_X Splitting	Q	Matrix shift
Free jet	15 132		(16 188)	1056*	15 766	
Ne	14 934	−198	15 951	1017	15 574	−192
N_2	14 773	−359	15 775	1002	15 328	−428
Ar	14 768	−364	15 753	985	15 309	−457
Kr	14 685	−447	15 655	970	15 182	−584
	14 670		15 624			
Xe	14 559	−573	15 475	916	15 035	−731
	14 518		15 412			
He	15 089	−43	(—)	1056*	15 703	−63
Shpol'skii	14 475	−657	15 332	857	14 914	−852
	14 411	−721	15 275	864	14 885	−881

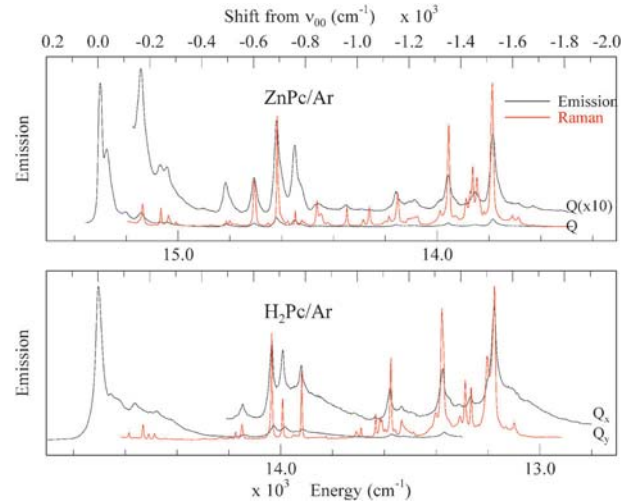

Fig. 3 A comparison of the fluorescence and Raman spectra of ZnPc (upper panel) and H_2Pc (lower panel) revealing the very strong similarities between the emission and Raman spectra. Emission spectra of ZnPc/Ar were excited in the Q band at $\lambda = 647.2$ nm. H_2Pc/Ar was excited in Q_Y at $\lambda = 637.9$ nm and excited in Q_X at $\lambda = 678.9$ nm. The scale on the top of both plots shows the emission energies as a shift from the position of the 0–0 transition. Conventional Raman spectra of ZnPc and H_2Pc in KBr pellets are shown by the red trace (ref. 24).

phthalocyanine do not exist in the spectrum of the metallophthalocyanine, especially in N_2.

2. Emission spectra

Only emission corresponding to transitions from $v' = 0$ in the first excited state [$Q(S_1)$ or $Q_X(S_1)$ in the case of ZnPc or H_2Pc respectively] to various vibrational levels v'' in the ground $G(S_0)$ electronic state was observed. Thus in the case of both molecules vibrationally relaxed emission occurs. In addition, similar emission was observed with laser excitation in the Q_X or Q_Y states of H_2Pc revealing that the non-radiative relaxation from Q_Y to Q_X is much faster than the $\sim$1 ns timescale of our experiment. The phonon broadened emission bands recorded for ZnPc in the present study, preclude a detailed analysis of either Jahn–Teller distortions or crystal field splitting in the excited state.

Fig. 3 provides a comparison of the emission spectra recorded for ZnPc and H_2Pc in an Ar matrix. Both molecules show a well-resolved vibronic structure extending from 0 to 1600 cm^{-1} from the origin of the electronic transition. It is evident that the emission spectra of the two molecules exhibit many similarities, especially the vibronic progression consisting of three dominant bands in the red part (1100 to 1500 cm^{-1} shifted from the origin) of the spectrum. The frequencies of the emission bands of ZnPc recorded in different solids are collected in Table 2, while they are given in Table 3 for H_2Pc in the same solids. For each species, the fluorescence intensity distribution of the vibronic structure is the same in all the matrices (and all the families of sites). It is also evident in Fig. 3 that the 0–0 transition dominates the emission intensity by more than a factor of 10. This is consistent with the results of measurements made in low temperature molecular beams[6,7]

Table 2 Frequencies (in cm^{-1}) of the vibrational levels of ground state [$G(S_0)$] ZnPc as measured in emission for different matrices. The Shpol'skii data is from Huang *et al.* [ref. 13] while the symmetry attributions are from ref. 24

Ne	N_2	Ar	Kr	Xe		Shpol'skii	DFT
	21	34	79		w		
	104	102	104	102	w	125	B_{2g}
	163	161	161	161	m		B_{1g}
	227	237	237		w	232	B_{2g}
	262	260	260	265	w		A_{1g}
495	488	490	491	488	m	482	B_{2g}
						536	B_{1g}
595(s)	597	598	598		m	592	A_{1g}
673	683	689	689		s	681	A_{1g}
751	752	751	751		s	750	B_{1g}
841	845	845	845		m	836	A_{1g}
956	945	945	945	954	w	950	B_{2g}
1151	1147	1150	1149	1152	m	1143	B_{1g}
	1215	1221	1221	1223	w		B_{2g}
1346	1346	1346	1346	1350	s	1342	A_{1g}/B_{1g}
1451	1448	1448	1448	1452	m		B_{1g}
1519	1525	1525	1524	1522	s	1518	B_{1g}
1614	—	1624	1610	1613	w		B_{2g}

in which the 0–0 transition was found to carry most of the Franck–Condon intensity.

When the laser excitation frequency is tuned inside the 0–0 band of the first excited state, the emission spectra show slight changes in terms of frequency shifts and the shapes of the vibronic bands. This is due to multiple site occupancy. Nevertheless, the fluorescence line narrowing effect is not strong because of a non-negligible coupling with the lattice phonons. In the case of ZnPc, two or three main families of sites are thus detected in all the matrices. Similarly, a limited number of families of sites were observed for H_2Pc, except in solid nitrogen where the number of clearly distinct families of

Table 3 Frequencies (in cm^{-1}) of the vibrational levels of ground state [$G(S_0)$] H_2Pc measured in emission for different matrices. The Shpol'skii data are from Huang *et al.* [ref. 13] and the gas data from Fitch *et al.* [ref. 8]. The symmetry attributions are from ref. 24

Gas phase	Ne	N_2	Ar	Kr	Xe		Shpol'skii	DFT
132		—	140	143	—	m	136	A_g
184		—	190	—	—	vw	184	B_{1g}
231		—	238	238	—	vw	232	A_g
484		—	489	494	—	vw	487	B_{1g}
544		—	—	544	—	vw	542	A_g
574		574	576	576	572	w	569	A_g
685	688w	687	688	688	682	s	683	A_g
729	726	731	730	731	727	s	725	A_g
768		—	—	771	—	vw	769	A_g
799		802	802	802	800	m	801	A_g
1012		—	—	—	965	vw	1009	A_g
1037		—	—	1031	1030	vw	1030	B_{1g}
1111	1070m	—	—	—	1090	vw	1107	B_{1g}
1144	1148	—	1145	1145	1143	m	1141	A_g
1189		—	1188	1190 (br.sh)	1184	w	1183/1188	A_g and/or B_{1g}
1233		—	—	—	1253	vw	1233	B_{1g}
1346		1356	1350	1351	1350	s	1352	A_g
1375	1383	—	—	—	1376	vw	1372	A_g
1456	1472	1460	1456	1456	1456	w	1453	A_g
1517		—	1523	—	—	vw	1522	A_g
	1535	—	—	—	—		1542/1546	A_g and/or B_{1g}
1545	1547	1553	1550	1550	1554	s	1555	A_g

sites is larger. However, while the Q_X state provides good site selective excitation, with narrow emission bands, excitation of the Q_Y state results in a much poorer site selection, as evident in emission by a broadening of bands in Ar (shown by the lower black trace in Fig. 3) or an additional structure involving multiple sites in nitrogen. This effect arises as a result of the spectral overlap of the absorption bands of the two electronic states in H_2Pc in this region.

3. Time-resolved emission

A summary of the emission decay curves recorded for H_2Pc and ZnPc isolated in different solids (N_2, Ar, Kr and Xe) is given in Fig. 4. The fluorescence decay curves were measured with time-gated iCCD detection and the lifetimes extracted by single exponential fits. From the timescales indicated in Fig. 4, the fluorescence lifetimes of H_2Pc are significantly longer than those of ZnPc. Thus the lifetimes of free base phthalocyanine are 12, 13, 13, 8 and 2.7 ns for Ne, N_2, Ar, Kr and Xe respectively, while the lifetimes measured for ZnPc in N_2, Ar and Kr all have very similar values around 3 ns. With an experimental uncertainty of ± 1 ns, the decay times in the lighter rare gases and nitrogen all agree and from their lack of temperature dependence, are not affected by any non-radiative relaxation induced by the matrix environment. These values are consistent with the lifetimes observed for porphyrins, such as zinc and free-base tetraphenyl porphine (ZnTPP and H_2TPP) in the gas phase.[32] The fluorescence lifetimes of H_2Pc and ZnPc are shortest in Xe ($\sim$2.8 ns) and Kr (8 ns), probably due to the competitive, non-radiative $S_1 \rightarrow T_1$ intersystem crossing—a transition enhanced in the heavier host solids. Attempts to observe the phosphorescence, predicted to occur in the near infrared (NIR), from the triplet states of H_2Pc and ZnPc in Xe with dye laser excitation of the Q state proved unsuccessful using both FT-NIR interferometer and NIR diode array dispersive detection methods.

4. Excitation spectra

The excitation spectra recorded for the phthalocyanines provide more highly resolved bands than what has been achieved in previous absorption studies. The results obtained for ZnPc and H_2Pc isolated in different matrices are shown in Fig. 5 and 6 respectively. To facilitate easy comparison of the data recorded in different environments, all the spectra presented are shown as the shift from the band origin (ν_{0-0}) of the Q_X state. The energies of the different modes of ZnPc for the major sites in Ar, Kr, Xe and N_2 (calculated as the shift from the band origin) are collected in Table 4 and compared with Shpol'skii matrix[13] and gas phase data.[6] The energies of the different vibronic modes observed for H_2Pc are collected in Table 5 and compared with Shpol'skii matrix[13] and gas phase data.[6,7]

The excitation spectra for ZnPc were not explored beyond 900 cm^{-1} from the band origin of the Q state for experimental reasons. As shown in Fig. 6, the spectra for H_2Pc are the same in all matrices up to $\sim$900 cm^{-1}, but differences appear at higher wavenumbers. The reason for this is the fact that the Q_Y state of H_2Pc, located around 1000 cm^{-1} from ν_{0-0} of Q_X, can induce a coupling with excited vibrational levels of the Q_X state—the electronic analogue of the Fermi resonance. Since the Q_X–Q_Y splitting depends on the matrix, as quoted in Table 1, the vibronic resonance will couple different excited state vibrational modes with the Q_Y state in different matrices. For the same reason, the coupling may be quite different for the different sites present in a single matrix.

IV. Discussion

A. Vibronic structure in emission

ZnPc and H_2Pc are large molecules exhibiting very many vibrational modes (165 and 168 respectively) but due to their high symmetry (D_{4h} and D_{2h} respectively) these modes can be

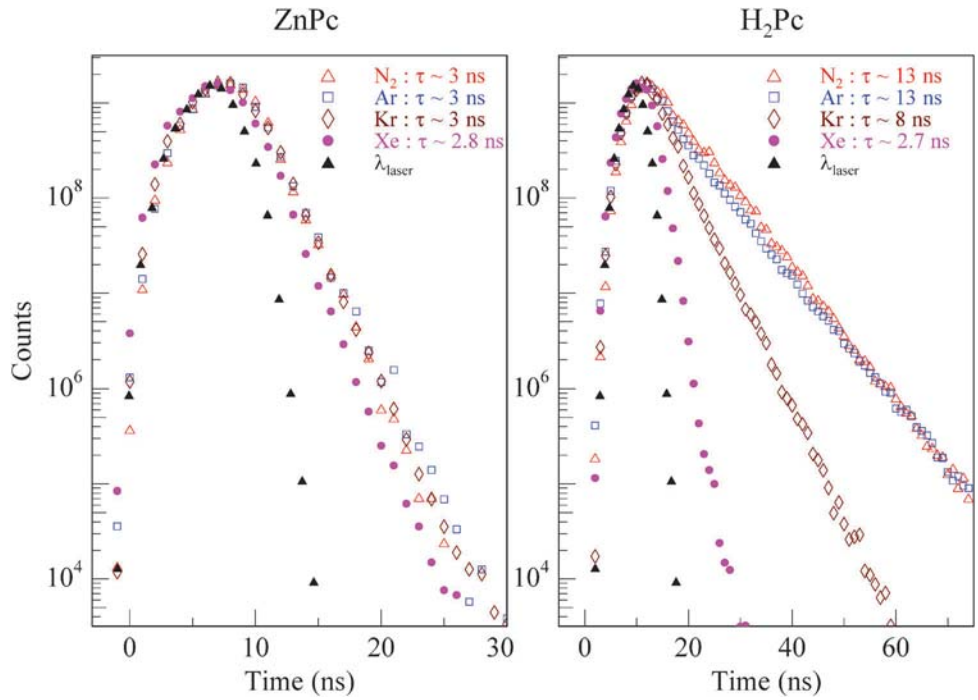

Fig. 4 Semilog plots of the emission decay curves extracted from time resolved emission spectra recorded at 13 K for ZnPc and H_2Pc isolated in a variety of low temperature matrices. The shape of the excitation pulse of the laser is also shown.

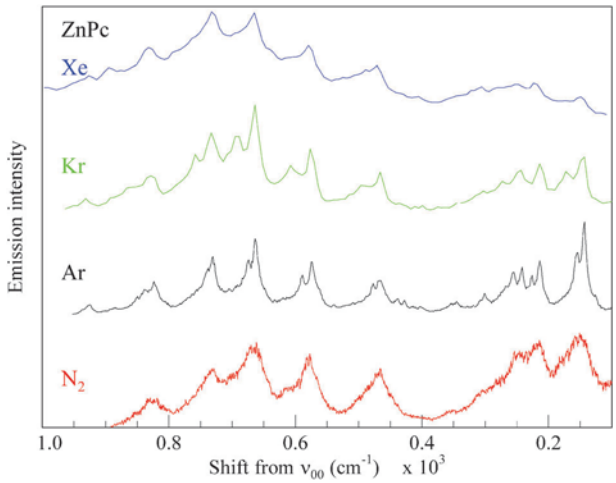

Fig. 5 A comparison of the fluorescence excitation spectra of ZnPc isolated in N_2, Ar, Kr and Xe recorded at $T = 13$ K by monitoring the emission corresponding to the vibrational level 1525 cm^{-1} from the band origin. All the data shown is presented as a shift from the band origin. The band structure reveals evidence for two distinct sites for ZnPc especially in Ar and Kr. The asymmetric shape on the blue side of most bands arises from phonon effects.

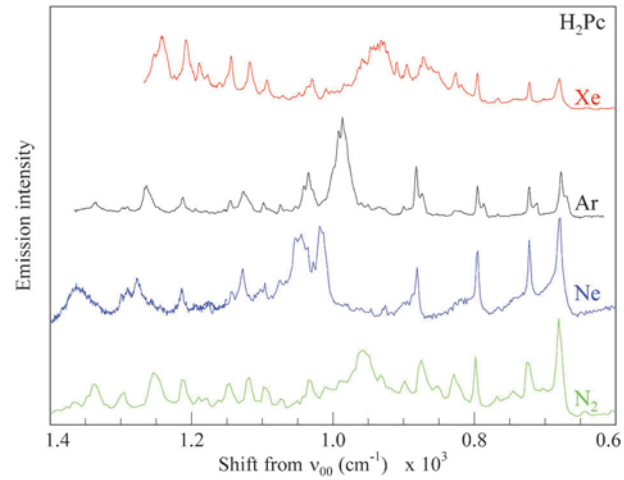

Fig. 6 A comparison of the fluorescence excitation spectra of H_2Pc isolated in Ne, Ar and Xe at $T = 8$ K recorded by monitoring the emission corresponding to the vibrational level 1550 cm^{-1} from the band origin. The N_2 data was obtained from the origin of the Q_X state. Particularly noteworthy in this plot is the similarity of the vibronic structure up to about 950 cm^{-1} from the band origin and the irregular nature of the structure present at higher energies. The doublet structure observed most clearly in Ar is due to the existence of a secondary site. The excitation spectrum shown for N_2 corresponds to the most blue site (14 859 cm^{-1}) in absorption. Excitation spectra of three other sites are presented in Fig. 9.

classified into a limited number of symmetry groups. A simplifying consequence of the high symmetry is that the number of modes which are infrared or Raman active is greatly reduced. Furthermore, as these molecules have a centre of inversion, there is mutual exclusion between the IR-active and Raman-active modes, as indicated by the vibrational representations. Selection rules will also reduce the number of vibrational modes involved in the electronic transitions.

The electronic $S_1 \leftrightarrow S_0$ transitions for both ZnPc and H_2Pc are fully allowed and in the Born–Oppenheimer approximation, only the totally symmetric (a_{1g} and a_g respectively) vibrational modes of these molecules should be observable in excitation or emission. Nevertheless, an efficient vibronic

Table 4 Wavenumbers of the observed bands in the excitation spectra of ZnPc trapped in N_2, Ar, Kr and Xe matrices. The values quoted are the shift from the band origins indicating the vibrational levels in the excited state. The gas phase values were published by Plows and Jones [ref. 6] while the Shpol'skii data is from Huang *et al.* [ref. 13]. The indicated symmetries were obtained from a comparison with those known from DFT results [ref. 24] in the ground state

symmetry DFT (G)	Gas phase	N_2	Ar	Kr	Xe	Shpol'skii
B_{2g}	103		87			
B_{1g}	153	164	154	155	155	
B_{2g}	226	229	225	224	227	
A_{1g}	256	259	252	253	255	
E_g	306		314	315	314	
E_g?	324		356			
E_g	419		412	410	410	
E_g?	430		439			
B_{2g}	482	479	478	476	479	477vs
B_{1g}	565					568w
A_{1g}	589	593	586	587	586	587vs
A_{1g}		676	675	675	671	673vs
B_{1g}		744	742	742	737	742s
A_{1g}		832	837	838	837	832m/839m
E_g?		846	851			851w
B_{2g}			940	942		937w

mixing[13] occurs between the S_1 state and the Soret states so that modes of other symmetries will appear in the spectra. For ZnPc whose $Q(S_1)$ state has ^1E_u symmetry, modes that transform as the a_{1g}, a_{2g}, b_{1g} and b_{2g} irreducible representations can induce this coupling. Similarly, the $Q_X(S_1)$ state of H_2Pc, which has $^1B_{3u}$ symmetry, will be coupled to the Soret states by a_g and b_{1g} modes. All these modes, except the a_{2g} modes of ZnPc, are Raman active modes. Additional modes which are Raman active are e_g modes in the D_{4h} group of symmetry and b_{2g} and b_{3g} modes in the D_{2h} group of symmetry. These modes correspond to out-of-plane vibrations in the cases of ZnPc and H_2Pc. In agreement with the experimental Raman results, our recent vibrational analysis of ZnPc and H_2Pc[24] found the intensities of the out-of-plane Raman-active modes to be very weak. So from symmetry considerations, strong similarities are expected between Raman and emission spectra.

The normal Raman spectra of ZnPc and H_2Pc recorded in KBr pellets with continuous-wave 532 nm excitation are shown in Fig. 3 by the red traces along with the emission recorded in Ar matrices (black traces). The vibrational frequencies measured for the Raman active modes of both

Table 5 Wavenumbers of the observed bands in the excitation spectra of H_2Pc trapped in Ne, N_2, Ar, Kr and Xe matrices. The values quoted are the shift from the band origins indicating the vibrational levels in the excited state. The gas phase values were published by Plows and Jones [ref. 6] with additional values (shown in italics) from Fitch *et al.* [ref. 7] while the Shpol'skii data is from Huang *et al.* [ref. 13]. The indicated symmetries were obtained from a comparison with those known from DFT results [ref. 24] in the ground state

Symmetry (G)	Gas phase	Ne	N_2	Ar	Kr	Xe	Shpol'skii
B_{1g}				87		86	
A_g	*127*		131	129		129	136
B_{1g}			179	175		172	—
A_g	*226*		229	228			231
B_{1g}	476	476	—				474
A_g	566	568	—				565
A_g	678	680	—	677		680	679
A_g	723	720	719	722		722	720
A_g		763	763	768 (vw)		766(vw)	779
A_g	794	793	794	795	795	795	799
			—		811	819	809/818
B_{1g}		822	824	828 (vw)	825(vw)	827	828
B_{1g}	887	880	877[a]	882	876(large)	861–872	890
			895[a]	900		895	900
			906			910	
		926(vw)	931	933 (vw)		928–932	933
			947	949 (vw)	946	946	
			957	960 (vw)	956	958	—
	978	979	1000–970[b]	987–991		983	982
A_g		1010	1010	1009 (vw)	1013	1016	1009
		1017					
B_{1g}	1025	1024	1028[a]	1034			1024/1027
	1030	1034	1037[a]	1041	1033	1030	1036
	1044	1043	1048	1052	1044	1048	
	1059	1051			1064		—
B_{1g}	1078	1074	1069[a]	1074	1081	1070	1083
B_{1g}	1086	1096	1092	1098	1111	1094	1109
A_g		1128	1119	1126	1128	1118	1115
A_g	1137	1142	1142	1144	1150	1143	1142
A_g		1178(vw)	1178		1176	1161(vw)	1156
A_g	*1184*		1189	1194 (vw)		1189	1180
B_{1g}	1221	1214	1214	1212	1213	1208	1205
			1254	1264	1251	1243	1239
A_g	1285	1278	1295	1291–1297	1285		1288
A_g	1334	1350	1339	1336	1353		1355

[a] Frequencies depending on the site: they decrease with increasing frequency of the site. [b] Main band with frequency depending on the site: its frequency decreases with increasing frequency of the site—see text and Fig. 9.

molecules have been presented and analysed by us.[24] What is most evident in Fig. 3 is the very strong similarity between the visible emission and the normal Raman spectra in the case of both molecules. Thus while there are some intensity differences between the emission and Raman spectra, the line positions all agree. The significance of this observation is that the mode assignments established by us[24] for the Raman bands can now be used to assign the bands present in the emission spectra.

The theoretically predicted Raman spectra of H_2Pc and ZnPc are compared with experimental Raman and fluorescence data in Fig. S1 and S2 respectively of the supplementary material provided. Assignment of the vibronic structure of the emission spectra is then possible using the ground state Raman results. The most prominent bands in the emission and Raman spectra are numbered in these figures and the mode assignments, taken from the DFT Raman predictions, are listed in Table 6 for ZnPc and H_2Pc, highlighting the similarities between both molecules. The most intense Raman active mode for ZnPc is predicted at 1526 cm^{-1} with b_{1g} symmetry, corresponding to an out-of-phase stretching of the C–N–C bonds in the tetrapyrrole ring. The corresponding mode is predicted at 1551 cm^{-1} for H_2Pc. It is noteworthy that the fluorescence bands at 1525 cm^{-1} for ZnPc and at 1550 cm^{-1} for H_2Pc, which exhibit[27] efficient stimulated emission (SE), are very close to the calculated frequency for the most intense Raman mode of both molecules. In more concentrated samples or under higher laser excitation intensity, two other modes have been observed to exhibit SE. This effect is especially prevalent in H_2Pc/N_2 samples where the modes at 730 cm^{-1} and 688 cm^{-1} also produce stimulated emission. These two modes are also quite intense in fluorescence and Raman spectra and both correspond to concerted motion of the inner-ring of the molecule. On the other hand, stimulated emission was also observed in free-base tetra-benzo porphine (H_2TBP) in Ar and H_2TBP/N_2 samples on a S_1–S_0 vibronic transition towards a vibrational excitation of H_2TBP in the ground state corresponding to an out-of-phase stretching of the C–C–C bonds in the internal ring, the analogue[28] of the 1550 cm^{-1} excitation of H_2Pc. This analysis provides the first information on the characteristics of the vibrations involved in SE.

The good agreement between the Raman and fluorescence frequencies was expected because of the similar selection rules, but the observed intensities in Raman and fluorescence spectra are also quite similar. This is consistent with the fact that all the vibronic transitions observed in fluorescence are transitions from $v_i' = 0$ to $v_f'' = 1$ for different vibrational modes, *i.e.* no overtones or progressions are present in the observed emission spectra.

B. ZnPc excitation spectra

Fig. 7 provides a comparison of the excitation and emission spectra recorded for zinc phthalocyanine in Ar. In this figure the emission spectrum has been reversed around the band origin of the $Q(S_1) \rightarrow G(S_0)$ transition for the purpose of comparison with the excitation and/or absorption spectra. The characteristic most evident in Fig. 7 is the mirror symmetry that exists between the excitation (red trace) and emission (blue trace) spectra as very well illustrated by the Ar data shown. The apparent weak intensity of the 0–0 band in excitation is an artefact due to strong re-absorption arising from the overlap between absorption and emission bands. The frequencies found for the vibronic modes in emission and excitation in a variety of matrices can be compared in Tables 2 and 4 respectively.

The same selection rules exist for the vibronic coupling of an electronic transition in both absorption and emission and since both transitions originate from the vibrationless levels, similar spectra arise. The observed similarities in the vibronic intensity

Table 6 Descriptions of the vibrational motion for the 17 most intense bands in the emission spectra of ZnPc and H_2Pc in Ar. The emission values are compared with the observed Raman data previously published by us [ref. 24]. The symmetry labels are from the same work and were obtained from large basis-set DFT calculations. The frequencies are given in wavenumber (cm^{-1}) units and all the observed Raman modes involve in-plane motions. The spectral precision in emission is around 4–5 cm^{-1} and is slightly better than this in Raman (1–2 cm^{-1}), however, the latter data were recorded at room temperature from in KBr pellets while the emission is Ar matrix data recorded at 10 K. The discrepancy is larger for ZnPc than for H_2Pc, because of the broadening of the emission bands

Band #	ZnPc Obs. Emiss.	Raman Observed	H_2Pc Obs. Emiss.	Raman Observed	Mode description
1	161	157 (B_{1g})	140	130 (A_g)	Bridging C–N–C sym. deformation
2	237	228 (B_{2g})	190	183 (B_{1g})	Bridging C–N–C asym. deformation
3	260	257 (A_{1g})	238	228 (A_g)	Central ring breathing
4	490	480 (B_{2g})	489	480 (B_{1g})	Aryl rocking & central ring def.
5	598	588 (A_{1g})	576	566 (A_g)	Aryl deformation/central ring breathing
6	689	677 (A_{1g})	688	680 (A_g)	Bridging C–N–C sym. def and aryl def
7	751	747 (B_{1g})	730	723 (A_g)	Pyrrole deformation and C–N–C rocking
8	845	830 (A_{1g})	802	796 (A_g)	Pyrrole & aryl C–C str.
9	945	946 (B_{2g})	1090	1081(B_{1g})	ZnPc asym CNC bend/H_2Pc N–H IPB
10	1004	1009 (A_{1g})	1006	1007 (A_g)	Sym.aryl C–H def
11	1150	1142 (B_{1g})	1145	1140 (A_g)	Aryl C–C str. and C–H def
12	1183	1183 (B_{1g})	1188	1181 (A_g)	C–H def on aryl ring
13	1221	1210 (B_{2g})	1228	1228 (B_{1g})	C–H def/ aryl def and N–H IPB
14	1346	1338 (A_{1g})	1350	1337 (A_g)	Aryl C–C str. and pyrrole C–C stretch
15	1448	1447 (B_{1g})	1456	1451 (A_g)	C–H def
16	1525	1507 (B_{1g})	1550	1540 (A_g)	Bridging C_α–N_m–C_α asym.str and sym str of the C_α–N_H–C_α bonds
17	1624	1608 (B_{2g})	1605	1616 (B_{1g})	Aryl ring deformation

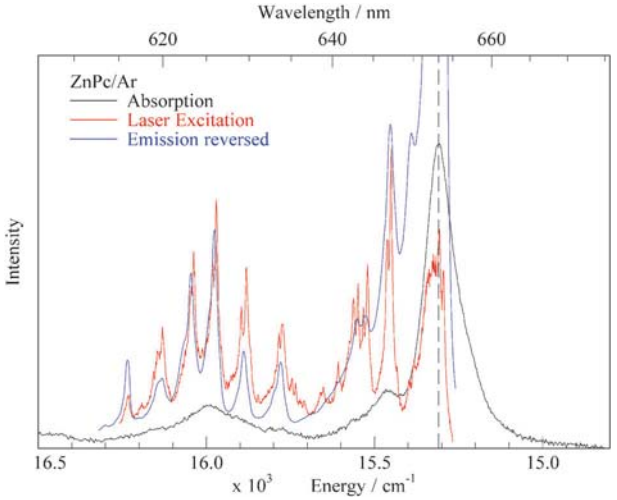

Fig. 7 A comparison of the absorption (black trace), excitation spectra and reversed emission spectra of ZnPc/Ar. Very good agreement exists between the excitation and reversed emission indicating immediately the strong mirror symmetry which exists between the two spectra. The dashed vertical line indicates the position of the band origin of the 0–0 transition at 15 309 cm^{-1} in the Ar matrix.

distributions in emission and excitation indicate that the geometry in this molecule is not greatly changed when in the first excited electronic state compared to the ground state. This is also confirmed by the fact that the 0–0 band is the most intense band in fluorescence spectra. Another key observation which can be made is that positions of the 0–0 transition in emission and excitation in all matrices agree to within the experimental error of our spectroscopic setups. Thus there is no Stokes shift on the Q state emission indicating very similar solvated geometries in the ground and first excited electronic states.

The vibrational frequencies of the two electronic states $G(S_0)$ and $Q(S_1)$ of ZnPc isolated in different matrices are in good agreement with the values obtained in Shpol'skii matrices[13] and those obtained in the gas phase[6] as shown in Tables 2 and 4 respectively. The discrepancy from mirror symmetry between excitation and emission noticed in Shpol'skii matrices[13] concerned the vibronic structure at higher energy. The absorption spectra recorded in the present study indicate this behaviour is not observed in matrices.

In the gas phase, 13 vibronic bands have been observed[6] in excitation for ZnPc ranging from 33 to 589 cm^{-1} from the band origin. As collected in Table 4 and shown in Fig. 5, all these modes have been observed for ZnPc in matrices at very similar energies except for the modes at 33, 103, 131 and 565 cm^{-1}. The last value corresponds to a weakly observed band in Shpol'skii matrices,[13] but the other values, corresponding to very weak bands, are not observed in any host, including helium droplets.[10] In matrices, the low frequency modes could be hidden in the phonon side band of the 0–0 band. The first clearly observed vibrational excitation is around 155 cm^{-1}. In jet-cooled experiments[6] the most intense band by far was the 0–0 transition, with this band at 153 cm^{-1} the second most intense in the spectrum. This is also what Lehnig *et al.*[10] observed in helium droplets. On the other hand, there are some discrepancies in the symmetry assignment of the vibrational bands between Plows' paper[6] and our results reported in Table 4 based on DFT calculations and a detailed comparison between the vibrational modes of ZnPc and H_2Pc.[24] Similar discrepancies occur between ref. 6 and Table 5 in the assignments of the vibrational levels of H_2Pc.

C. H_2Pc excitation spectra

1. General remarks. In contrast to ZnPc, a breakdown of the mirror symmetry occurs in excitation and emission spectra of H_2Pc around 1000 cm^{-1} above the band origin, ν_{0-0}, (Table 3 and 5 respectively) as illustrated in Fig. 8 for the case of H_2Pc in Ar. As revealed in Fig. 8, there is very good agreement between excitation and emission up to 800 cm^{-1} (energy around 15 600 cm^{-1}) above the origin of the Q_X state. Beyond this value, there is a pronounced lack of mirror symmetry where a gap exists in the emission frequencies, while broad strong bands appear in this range in excitation. This difference in vibronic structure between emission and excitation arises because of the existence of the $Q_Y(S_2)$ state at $\sim$1000 cm^{-1} from the $Q_X(S_1)$ state, which is not present in ZnPc. It is expected that excited vibrational levels of the Q_X state will be situated in the same region as the band origin of the electronic $Q_Y \leftarrow G$ transition. When coupling occurs between the two electronic states, the vibronic lines of the $Q_X \leftarrow G$ transition increase in intensity and are shifted-the vibronic analogue of Fermi resonance.[33] The oscillator strength of the $Q_Y \leftarrow G$ transition is then distributed among a number of vibronic $Q_X \leftarrow G$ transitions rendering the exact position of the band origin of Q_Y difficult to determine.

When the manifold of the Q_X state vibronic levels in resonance with the origin of Q_Y is not dense, and the vibrational structure is well resolved, the band origin of the latter

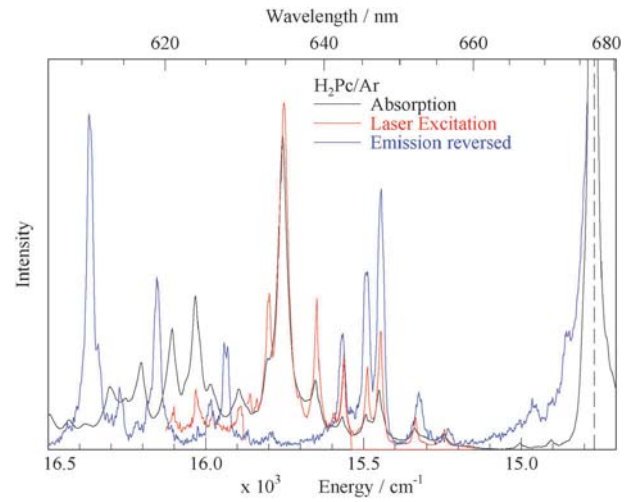

Fig. 8 Same comparison as presented in Fig. 7 but for H_2Pc/Ar data. It is evident in this plot that the vibronic structure up to about 950 cm^{-1} from the band origin are similar in emission and excitation but that the latter becomes irregular at higher energies. Particularly noteworthy are the intense bands which are present in the excitation in the region of 1000 cm^{-1} but which are absent in emission. The dashed vertical line indicates the position of the 0–0 transition at 14 768 cm^{-1} in solid Ar.

can be distinguished in the spectra. This condition existed in the low temperature spectra recorded by Arabei *et al.*[34] in the case of H_2TBP in *n*-alkane crystals. In contrast when this manifold is very dense, direct line-to-line assignment is not possible and the energy of the Q_Y state is estimated from a band analysis[33,35] involving deconvolution of conglomerates of bands. In the case of H_2Pc, the energies of modes with the right (b_{1g}) symmetry for efficient coupling between the Q_X and Q_Y states are now known from recent DFT results[24] and are shown in Fig. 10 for fundamentals and combination of pairs. As indicated in the figure, the Q_X–Q_Y energy gap is in an energy range where very few fundamental b_{1g} modes exist.

2. Matrix and site effects on the Q_X/Q_Y state couplings. The Q_X–Q_Y splitting of H_2Pc is matrix dependent as is evident in the absorption and excitation spectra presented in Fig. 2 and 6 respectively (see Table 1 for values). As a result, different vibronic bands of Q_X will couple with the band origin of the Q_Y state with different coupling strengths. Furthermore, it is also to be expected that distinct sites in the same matrix may exhibit different Q_X–Q_Y splittings. This phenomenon has already been observed for other porphyrins (*meso*-tetra-azaporphine, *meso*-tetrapropyl-porphine and tetrabenzo-porphine) in Shpol'skii matrices.[33,35] In the case of H_2Pc, this effect can be followed very well in nitrogen matrices which present many different sites of isolation as illustrated in the panels on the right of Fig. 9.

Table 1 reveals the decrease in energy of the Q_X origin from the gas phase to xenon matrices through He droplets, Ne, N_2, Ar and Kr hosts successively. The Q_X–Q_Y splitting follows qualitatively the same host dependence, decreasing from the gas phase to Xe matrices. It is known from Huang's results[13] in Shpol'skii matrices that an even smaller G-Q_X transition energy exists in *n*-decane than in Xe together with a reduced splitting between the Q_X and Q_Y states. In gas phase jet experiments, Fitch *et al.*[7] identified the origin of the Q_Y state around 16 700 cm^{-1}, due to a large intensity increase of congested bands in this spectral region. More recently, Plows and Jones[6] reported the onset of the Q_Y band around 1000 cm^{-1} above the Q_X origin. The latter assignment is in good agreement with the results on H_2Pc in helium droplets.[10] Moreover, Fitch *et al.*[8] observed in their jet experiments a large broadening of fluorescence bands when exciting H_2Pc at 16 188 cm^{-1}, *i.e.* 1056 cm^{-1} above the Q_X origin, which could be correlated to an excitation of a coupled Q_X–Q_Y vibronic band. As this band is the most intense in this spectral range, it can be assigned in a first approximation to the origin of the Q_Y state in the gas phase. From the work of Fitch *et al.*[8] and Lehnig *et al.*,[10] it seems that the Q_X–Q_Y splitting is not modified appreciably by the helium droplet environment. The least perturbing matrix host is neon, and effectively, the excitation band pattern in this host (shown in Fig. 9) remains very similar to the case of He around the Q_Y origin, involving the same vibronic levels.

According to the DFT results[24] shown in Fig. 10, only three fundamental b_{1g} modes exist in the 1000–1100 cm^{-1} spectral range in the ground state. These modes have been observed[24] in Raman spectra at 1026, 1081 and 1099 cm^{-1}. The same modes appear in the excitation spectra of H_2Pc in the jet experiments[7] together with a few other weak bands coming from the interaction of Q_X modes *via* interstate coupling with the Q_Y origin. Whereas all these modes appear also in the excitation spectra of H_2Pc isolated in Ne, their intensity

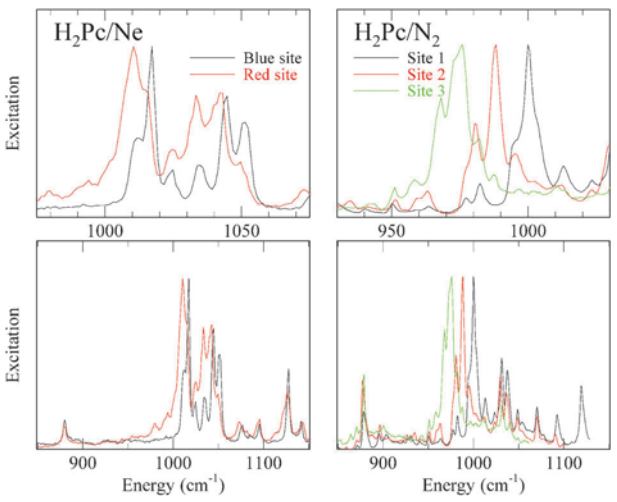

Fig. 9 Detail of the excitation spectra in the region where coupling can occur between the band origin of the Q_Y state and excited vibrational levels of Q_X. The data presented was recorded in neon (left panel) and nitrogen (right) by monitoring emission of the band origin of the Q_X–G transition. All the spectra are shown relative to the bands origin of the Q_X state. In Ne the blue and red sites are located at 15 007 and 14 934 cm^{-1} respectively while sites 1, 2 and 3 in N_2 are at 14 761, 14 787 and 14 832 cm^{-1} respectively. Most evident in this comparison is the relatively simple structure present in N_2 and the much more complex bands in Ne.

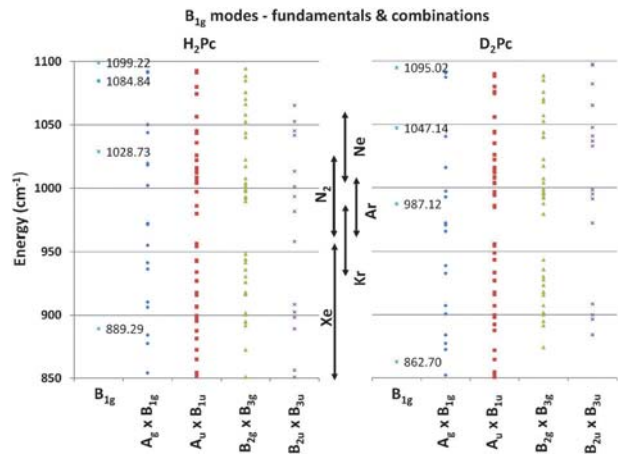

Fig. 10 An energy level diagram showing the vibrational modes of H_2Pc and D_2Pc with the correct symmetry (b_{1g}) to couple the Q_X and Q_Y electronic states in the region of the band origin of the Q_Y state. Fundamental B_{1g} modes are shown with frequencies in wavenumber units. The combinations modes shown are limited to just pairs of modes. The frequencies of both the fundamental and combination bands were determined in recent (scaled) DFT calculations [ref. 24]. The vertical arrows shown in the central region of the plot are the energy ranges of the Q_Y state band origin for the sites present in Ar, Kr and N_2 while those shown for Ne and Xe are the ranges observed for the complex band structures present in the region of the band origin of the Q_Y state in these two hosts.

distribution is different from that in the gas phase or in He droplets. In Ne, the most intense band is, as shown in the upper left of Fig. 9, between 1001 and 1017 cm^{-1}, depending on the site (see later), with also large intensities in the bands around 1045 cm^{-1}. We conclude that the Q_X–Q_Y splitting is reduced by 40 cm^{-1} in Ne, with a possible interaction between the fundamental 1026 cm^{-1} (value from Raman spectra) b_{1g} mode and the Q_Y state origin. This coupling could explain the intensity distribution over a larger number of main bands in neon.

From our ground state DFT study[24] there are no fundamental b_{1g} modes between 1026 cm^{-1} and 889 cm^{-1}. The Q_X–Q_Y splitting reaches this range in the heavier inert gas matrices and consistent with this, the excitation spectra in Ar, Kr and N_2 show simpler maxima between 950 and 1000 cm^{-1} above the Q_X origin. The exact values depend on the host and the site but these maxima can be taken directly as the Q_Y state origins. In contrast, excitation spectra in Xe show complex structures between 850 cm^{-1} and 950 cm^{-1}. Obviously, this structure is the result of a more extensive coupling between the Q_Y origin and the vibrationally excited levels of Q_X, involving a larger number of vibrational states as observed for neon.

In Xe the b_{1g} mode of Q_X around 889 cm^{-1} is close to resonance with the Q_Y origin. One can notice that this particular mode is totally absent in emission spectra whereas it is observed in excitation in all the cases, including in the gas phase. Its intensity enhancement comes from the Q_X/Q_Y state coupling. Table 5 reports the frequency values of the bands observed in excitation spectra in different hosts. Even when the values do not correspond to simple vibrational levels of Q_X, they are not very different from one host to another. This means that in all the cases, the same vibronic levels are involved in the Q_X/Q_Y coupling, and that this coupling remains weak.

As the energy of the Q_Y state also shifts for different sites within a given matrix, different modes can couple with different interaction strengths, producing quite distinct bandshapes. In Fig. 9 a detailed comparison of the band origin of the Q_Y state of H_2Pc in Ne and N_2 is shown for spectrally well defined sites. The data is presented as the shift from the band origin of the Q_X state and it is evident in the wider range scans presented in the lower panel, that the vibronic bands of the Q_X state match exactly while the origins of the Q_Y state differ by at least 10 cm^{-1}. In the upper panel it is also very evident that the Q_Y state structures are quite distinct in the two matrices. As shown on the upper left in Fig. 9 the two sites in Ne (labelled Red and Blue) are broad and appear as a pair of dominant bands, while the data shown for three sites in N_2 are simpler, appearing as single dominant band. This contrasting behaviour is attributed to the different Q_X/Q_Y state couplings which are energy dependent, as explained previously. The additional structure, clearly observed in excitation spectra of the most intense bands related to the Q_Y state, can come from the usual mismatch between the family of sites selected through its emission frequency, *i.e.* by its G-Q_X transition energy, and families of sites selected on another electronic transition, such as the G-Q_Y transition. In nitrogen matrices, where the main "Q_Y" band origin shifts progressively from one site to another, a similar shift is also observed on some other bands (distinguished by a and b in Table 5): these bands probably correspond to stronger Q_X–Q_Y vibronic coupling (Q_X vibrations of b_{1g} symmetry).

The transition energies of the red and blue sites of H_2Pc in neon differ by around 70 cm^{-1} in the Q_X–G band origins. With an additional shift of 10 cm^{-1} from one site to another, they differ by around 80 cm^{-1} in the Q_Y state origins. In nitrogen matrices, the two extreme sites shown in Fig. 9 differ also by around 70 cm^{-1} in the Q_X origins. However, due to an inverse trend in the Q_X–Q_Y splittings, they differ by only around 40 cm^{-1} in Q_Y origins. This inversion was observed, but more pronounced in the recent work by Arabei *et al.*[35] on methylated dibenzoporphin and was attributed to the different interactions between N–H H–N bonds and the lattice. This interaction is weaker in neon than in nitrogen. The observed inversion in nitrogen explains also a narrower Q_Y band than Q_X in absorption (see Fig. 2).

3. Effect of isotope substitution on the Q_X/Q_Y state couplings. The present analysis allows some comments to be made of the previous matrix study of H_2Pc in argon reported by Bondybey and English.[18] First of all, the polarisation behaviour of the excitation bands these authors present is in perfect agreement with the present assignments of the bands in terms of symmetries deduced from DFT calculations. Thus the a_g vibrational modes are observed[18] as parallel polarised bands while the b_{1g} modes are the perpendicular bands. These authors also identified an important deuteration effect in the excitation spectra of H_2Pc and D_2Pc in argon. The intense band assigned to the origin of the Q_Y electronic transition at 983 cm^{-1} (from the 0–0 of the Q_X-G transition) in H_2Pc was seen to be replaced by a complex structure with the most intense part, shifted down by 37 cm^{-1} to 946 cm^{-1} in D_2Pc. From our DFT results,[24] it is known that b_{1g} modes located between 800 cm^{-1} and 1100 cm^{-1} are those exhibiting the most pronounced isotopic effect, because they involve NH in-plane bending motions. In particular, the 1026 cm^{-1} mode (Raman value) appearing in the excitation spectra of H_2Pc around 1030 cm^{-1} in all the matrices, shifts to 986 cm^{-1} (Raman value) in D_2Pc. The corresponding D_2Pc unperturbed vibrational level at 987.12 cm^{-1} (scaled DFT Raman value) should, as shown on the right in Fig. 10 be in perfect resonance with the Q_Y origin in Ar, following our previous assignment in H_2Pc. The consequent strong Q_X/Q_Y interaction could explain the observed feature in D_2Pc/Ar samples with two intense bands distributed below and above the H_2Pc Q_Y origin energy.

The intense band shown in Fig. 8 at 882 cm^{-1} in the Ar excitation spectra (889 cm^{-1} Raman value) is considerably weaker in D_2Pc. The corresponding D_2Pc Raman value is calculated at 747 cm^{-1} but was not observed. This D_2Pc value, far from the expected Q_X–Q_Y splitting in Ar, could explain its loss of activity through the vibronic Q_X/Q_Y interaction. These modes involve a N–H(D) bending motion coupled to the bridging atoms C–N–C and peripheral aryl C–C–C atoms. Accordingly, it is not surprising that such modes are important in the Q_X/Q_Y coupling. Other modes at higher energies than the Q_Y state were also noticed to shift upon deuteration but due to the complex overlap of Q_X and Q_Y vibronic bands in this region, assignments are not straightforward. No isotopic dependence was seen for the vibronic bands in the excitation spectra up to and including the mode at 795 cm^{-1} from the Q_X state band origin.

V. Conclusions

We have investigated the electronic spectra of two tetrapyrrolic molecules isolated in rare gas and nitrogen matrices, namely free-base phthalocyanine and zinc phthalocyanine. A comparison of the Raman and fluorescence spectra for both molecules reveals striking similarities, not only in the band positions but also in the intensities. This behaviour is explained by the selection rules pertaining for both types of transitions in these planar molecules. This allowed the use of the assigned Raman active modes, calculated for the ground electronic state with large basis set, density functional theory, to identify the vibronic modes present in emission for H_2Pc and ZnPc. The observed vibronic frequencies in the ground (G) and first excited (Q) states of ZnPc were found to be very similar. This indicates a very similar geometry in the excited state to that in the ground state and allowed the vibrational modes in the Q state to be assigned using the DFT calculated Raman spectra. In the case of H_2Pc, the existence of the second excited Q_Y state only 1000 cm^{-1} above Q_X is responsible for the observation of a very complicated excitation spectrum due to coupling between the band origin of the $Q_Y(S_2)$ electronic state and vibrational levels of the $Q_X(S_1)$ state. This made assignment of the modes above the Q_Y more difficult using the ground state vibrational modes observed in emission or Raman spectra.

The energy difference between the Q_X and Q_Y states of H_2Pc was found to be dependent on the host matrix, with the largest Q_X–Q_Y splitting of 1017 cm^{-1} found in Ne and the smallest splitting of 916 cm^{-1} in Xe (mean values from absorption spectra). Consequently, the excitation spectra of H_2Pc strongly differ in band structures and energy distribution in the spectral range of the Q_Y origin from one host to the other and even from one trapping site to another in the same host. The non-adiabatic coupling of this band with fundamental b_{1g} modes of Q_X involving in-plane NH bending motions seems to be specifically important. Such couplings also explain the deuteration effect observed by Bondybey *et al.*[18] on the excitation spectra of the free-base phthalocyanines. Further analysis, including more extensive experimental analysis and theoretical calculations, is required in order to fully resolve the vibrational modes coupling in both excited states of H_2Pc and in various host environments.

Acknowledgements

This work was supported by the Ulysses France-Ireland research exchange grants (2006 and 2011) and the Science Foundation Ireland (SFI), Research Frontiers Programme (06/RFP/CHP012) Grant. The authors wish to acknowledge fruitful discussions with Professor S.M. Arabei.

References

1 F. M. Moser and A. L. Thomas, *Phthalocyanine Compounds*, Reinhold Publishing corporation, New-York, 1969.
2 T. Hanada, H. Takiguchi, Y. Okada, Y. Yoshida, N. Tanigaki and K. Yase, *J. Cryst. Growth*, 1999, **204**(3), 307.
3 J. L. Bredas, C. Adant, P. Tackx and A. Persoons, *Chem. Rev.*, 1994, **94**(1), 243.
4 D. Eastwood, L. Edwards, M. Gouterman and J. Steinfeld, *J. Mol. Spectrosc.*, 1966, **20**(4), 381.
5 L. Edwards and M. Gouterman, *J. Mol. Spectrosc.*, 1970, **33**, 292.
6 F. L. Plows and A. C. Jones, *J. Mol. Spectrosc.*, 1999, **194**(2), 163.
7 P. S. H. Fitch, Ch. A. Hayman and D. H. Levy, *J. Chem. Phys.*, 1980, **73**, 1064.
8 P. S. H. Fitch, Ch. A. Hayman and D. H. Levy, *J. Chem. Phys.*, 1981, **74**, 6612.
9 A. Slenczka, B. Dick, M. Hartmann and J. P. Toennies, *J. Chem. Phys.*, 2001, **115**, 10199; M. Hartmann, A. Lindinger, J. P. Toennies and A. F. Vilesov, *Phys. Chem. Chem. Phys.*, 2002, **4**, 4839; R. Lehnig, J. Sebree and A. Slenczka, *J. Phys. Chem. A*, 2007, **111**, 7576.
10 R. Lehnig and A. Slenczka, *J. Chem. Phys.*, 2003, **118**, 8256; R. Lehnig and A. Slenczka, *J. Chem. Phys.*, 2004, **120**, 5064; R. Lehnig, M. Slipchenko, S. Kuma, T. Momose, B. Sartakov and A. Vilesov, *J. Chem. Phys.*, 2004, **121**, 9396.
11 A. Stendal, U. Beckers, S. Wilbrandt, O. Stenzel and C. von Borczyskowski, *J. Phys. B: At., Mol. Opt. Phys.*, 1996, **29**, 2589.
12 J. Hala, I. Pelant, L. Parma and K. Vacek, *Czech. J. Phys.*, 1982, **32**, 705.
13 T.-H. Huang, K. E. Rieckhoff and E. M. Voigt, *J. Chem. Phys.*, 1982, **77**, 3424.
14 R. I. Personov, *Opt. Spectrosc.*, 1963, **15**, 30.
15 P. Geissinger and D. Haarer, *Chem. Phys. Lett.*, 1992, **197**, 175.
16 B. J. Prince, B. E. Williamson and R. J. Reeves, *J. Lumin.*, 2001, **93**, 293.
17 L. Bajema, M. Gouterman and B. Meyer, *J. Mol. Spectrosc.*, 1968, **27**, 225.
18 V. E. Bondybey and J. H. English, *J. Am. Chem. Soc.*, 1979, **101**, 3446.
19 D. H. Metcalf, T. C. vanCott, S. W. Snyder, P. N. Schatz and B. E. Williamson, *J. Phys. Chem.*, 1990, **94**, 2828.
20 R. Aroca, D. P. DiLella and R. O. Loutfi, *J. Phys. Chem. Solids*, 1982, **43**, 707.
21 D. R. Tackley, G. Dent and W. E. Smith, *Phys. Chem. Chem. Phys.*, 2001, **3**, 1419.
22 D. R. Tackley, G. Dent and W. E. Smith, *Phys. Chem. Chem. Phys.*, 2000, **2**, 3949.
23 X. Zhang, Y. Zhang and J. Jiang, *Vib. Spectrosc.*, 2003, **33**(1–2), 153.
24 C. Murray, N. Dozova, S. FitzGerald, J. G. McCaffrey, N. Shafizadeh and C. Crépin, *Phys. Chem. Chem. Phys.*, 2010, **12**, 10406.
25 S. G. Bown, C. J. Tralau, P. D. Coleridge Smith, D. Akdemir and T. J Wieman, *Br. J. Cancer*, 1986, **54**(1), 43.
26 P. Geissinger, L. Kaldor and D. Haarer, *Phys. Rev. B: Condens. Matter*, 1996, **53**, 4356.
27 N. Dozova, C. Murray, J. G. McCaffrey, N. Shafizadeh and C. Crépin, *Phys. Chem. Chem. Phys.*, 2008, **10**, 2167.
28 C. Crépin, N. Shafizadeh, W. Chin, J.-P. Galaup, J. G. McCaffrey and S. M. Arabei, *Low Temp. Phys.*, 2010, **36**, 451.
29 M. A. Collier and J. G. McCaffrey, *J. Chem. Phys.*, 2005, **122**, 184507.
30 C. Gée, A. Cuisset, L. Divay and C. Crépin, *J. Chem. Phys.*, 2002, **116**, 4993.
31 J. G. Radziszewski, J. Waluk and J. Michl, *Chem. Phys.*, 1989, **136**, 165.
32 U. Even, J. Magen, J. Jortner, J. Friedman and H. Levanon, *J. Chem. Phys.*, 1982, **77**, 4374.
33 S. M. Arabei, V. A. Kuzmitsky and K. N. Solovyov, *Opt. Spectrosc.*, 2007, **102**, 692.
34 S. M. Arabei, K. N. Solovev and Yu. I. Tatulchenkov, *Opt. Spectrosc.*, 1992, **73**, 406.
35 S. M. Arabei, V. A. Kuzmitsky and K. N. Solovyov, *Chem. Phys.*, 2008, **352**, 197.

